

The Cosmological Mass Function with 1D Gravity

Pierluigi Monaco

Institute of Astronomy, University of Cambridge, Madingley Road, Cambridge CB3 0HA – GB
Dipartimento di Astronomia, Università di Trieste, via Tiepolo 11, 34131 Trieste – Italy
email monaco@ast.cam.ac.uk

Giuseppe Murante

Dipartimento di Fisica, Università di Milano, Via Celoria 16, 20133 Milano – Italy
email Giuseppe.Murante@uni.mi.astro.it

(November 11, 2018)

The cosmological mass function problem is analyzed in full detail in the case of 1D gravity, with analytical, semi-analytical and numerical techniques. The extended Press & Schechter [1] theory is improved by detailing the relation between smoothing radius and mass of the objects. This is done by introducing in the formalism the concept of a growth curve for the objects. The predictions of the extended Press & Schechter theory are compared to large N-body simulations of flat expanding 1D universes with scale-free power spectra of primordial perturbations. The collapsed objects in the simulations are located with a clump-finding algorithm designed to find regions that have undergone orbit crossing or that are in the multi-stream regime (these are different as an effect of the finite size of the multi-stream regions). It is found that the semi-analytical mass function theory, which has no free parameters, is able to recover the properties of collapsed objects both statistically and object by object. In particular, the predictions of regions in orbit crossing are optimized by the use of Gaussian filtering, while the use of sharp k -space filtering apparently allows to reproduce the larger multi-stream regions. The mass function theory does not reproduce well the clumps found with the standard friends-of-friends algorithm; however, the performance of this algorithm has not been thoroughly tested in the 1D cosmology. Our preliminary analyses of the 3D case confirms that the techniques developed in this paper are precious in understanding the cosmological mass function problem in 3D.

98.80.-k 95.35.+d 98.65.Dx

I. INTRODUCTION

The most widely accepted view of the formation and evolution of the Large Scale Structure of the Universe (LSS) is currently based upon the gravitational instability of a self-gravitating density field. Such a density field should be dominated by non baryonic, collisionless dark matter [2]. The density field is supposed to be homogeneous, apart from small random Gaussian fluctuations which trigger the instability. The evolution of these fluctuations under the action of self-gravity is described by the Vlasov-Poisson equations [3]. Analytical approaches, typically linear or (Lagrangian or Eulerian) perturbative approximations, are able to reproduce the evolution of the matter field to the fully-developed non-linear stage only in case of special symmetries. Otherwise the validity of perturbative approaches is limited to the linear or so-called mildly non-linear regimes, when the evolution is still laminar and no *orbit crossing*¹ has occurred.

The evolution of the density fluctuations in the highly non-linear regime is usually described by means of large numerical simulations, in which the density field is sampled by massive particles accelerating according to their Newtonian gravitational force. These numerical N-body simulations, which are affected by severe numerical resolution limits, are able to provide final configurations which are not trivial to analyze and understand in detail. A joint use of numerical simulations and analytical approximations seems the best way to deepen our understanding of the gravitational problem in cosmology.

It is well known that a density field with random (Gaussian distributed) small perturbations gives birth to a hierarchy of collapsed, relaxed structures. One important quantity which characterizes the properties of these collapsed structures is the distribution of their masses, usually called the mass function (hereafter MF). An accurate MF theory

¹Orbit crossing is said to take place when two or more infinitesimal matter elements flow from different Lagrangian position to the same Eulerian coordinate.

is the starting point for modeling the statistical behavior of most cosmological objects, and can be extended to give predictions of the main properties of dark-matter structures.

The MF problem has been recently reviewed by Monaco (1998) [4]. While most predictions, since the one of Press & Schechter (1974 [1], hereafter PS; but see also Doroshkevich 1967 [5]), were based on heuristic extrapolations of linear theory, it is possible to construct a MF theory based on the powerful Lagrangian perturbation theory [6–9]; this is shown in Monaco (1997a,b) [10,11]. A key point is that the same basic concepts of collapse and of total mass of an object are not well defined. Collapse may be confused with total or partial virialization, and the total mass of the objects is usually estimated through order-of-magnitude arguments. Within the Lagrangian perturbation framework, it is possible to define collapse in a precise way, i.e. as orbit crossing (hereafter OC) of mass elements. In 3D, this definition does not distinguish between just-collapsed structures, like two-dimensional or one-dimensional transients (‘pancakes’ or ‘filaments’), and fully virialized clumps. It is then appropriate to compare theory and numerical simulations in terms of regions which have undergone OC, then checking the relation between these and the collapsed clumps found with other, more standard algorithms. Besides, the problem of a clear definition of the total mass of a structure is of a geometrical nature. It is necessary to determine the volume and topology of those extended regions that share the property of ‘being collapsed’. We will propose in this paper a simple and effective way to address this problem.

As an intermediate step to the full solution of the MF problem, it is convenient to analyze a simplified case, that of 1D gravity. While being a purely academic problem, 1D gravity provides a valuable gymnasium in which to develop and test analytical predictions. The 1D problem was already analyzed, in the framework of the adhesion theory [15], by Doroshkevich & Kotok (1990) [16] and by Williams et al. (1991) [17], while Doroshkevich et al. (1980) [13] studied the problem with N-body simulations. From the dynamical point of view, the geometry of first collapse (which coincides with OC) is predicted to be 1D, or pancake-like [18,19] (see in particular Shandarin et al. 1995 [20]), so 1D is the relevant restricted case, especially when OC is used as collapse definition. As will be discussed in Section II.A, Lagrangian perturbation theory is trivial in 1D because the first-order Zel’dovich approximation is exact up to OC [19]. By comparing theory with simulations, it is then possible to test the elements which are missed by this approach, without taking into account the effects of the truncation of the perturbative series. The geometry of the 1D structures is highly simplified because connected regions are just segments. The statistics of collapsed regions are also greatly simplified. It will be shown in Section II.A that the statistics of collapsed regions can be based on a Gaussian field, although the gravitational evolution of perturbations induces strong non-Gaussianities in the density distribution.

Anyway, the MF problem in 1D is not trivial and presents many complications relevant to the 3D problem. The reason why the MF problem can benefit from a 1D analysis is that it is, in some sense, 1D by itself. It was shown by Monaco (1997b) [11] that, in the general case in which the non-linear and non-local gravitational dynamics are taken into account, the MF problem can be formulated in terms of an infinite-dimensional diffusion system (see Section II.B for more details) that can be ‘projected’ onto one dimension and solved as a random walk with white or colored noise (Peacock & Heavens 1990, hereafter PH [21]; Bond et al. 1991 [22]). Also the merging histories of dark-matter halos are commonly found by solving a 1D diffusion equation (Bond et al. 1991 [22]; Lacey & Cole 1993 [23]). This reflects the fact that only a limited amount of information is present in the MF, to the extent that limited information on a structure is given by its mass. The clustering of collapsed halos, for instance, requires knowledge of the space correlations [24], and thus would not benefit much from a 1D analysis. The utility of the results of this paper for a 3D analysis of the mass function problem will be discussed in the Conclusions.

The scope of this paper is to give a complete approximated solution of the MF problem in 1D, and to compare it to the results of numerical simulations. The concepts and techniques developed here can be adapted to the full 3D case; this will be discussed at the end of Section V. The plan of the paper is the following. In Section II the analytical theory of the 1D MF is presented: the excursion set approach is reviewed, and the concepts of the *collapse radius* field and of the *growth curve* for the objects is introduced. Section III describes the N-body simulations, based on a PM code, and the multi-scale algorithm with which the OC regions are found. The distinction between points that have a negative Jacobian and those that are in multi-stream regions is clarified. Section IV presents the results of the comparison of theory and simulations. The comparison is based both on the collapse radius fields and on the collapsed objects. Section V gives a summary of the main results and the conclusions.

II. ANALYTICAL THEORY

As this 1D analysis is meant to provide tools for addressing the complex 3D problem, it is useful to consider a 1D universe whose background geometry is that of a 3D Friedmann model. This is achieved by considering a Friedmann universe with purely planar perturbations, i.e., homogeneous infinitely extended parallel planes interacting via self-

gravitational force. The evolution of these perturbations is then 1D. As the non-linear evolution of perturbations is easily disentangled from the evolution of the background geometry (see, e.g., Monaco 1998 [4]), all the analyses presented in this paper are restricted to the case of an Einstein-de Sitter model, in which the geometry is globally flat and the expansion is described by the scale factor $a(t) \propto t^{2/3}$ (when the universe is dominated by pressureless matter). The 3D background density $\bar{\rho}_{3D}$ is equal to the critical one, $\bar{\rho}_{3D}(t) = 3H^2(t)/8\pi G$, where G is the gravitational constant and $H(t) = \dot{a}(t)/a(t)$ is the Hubble parameter [3]. The density parameter Ω is defined as the ratio between the background density $\bar{\rho}_{3D}$ and the critical density; in the Einstein-de Sitter model $\Omega = 1$. The matter field is denoted by $\varrho(x)$ (mass per unit length), the 1D background density as $\bar{\varrho}$ (equal to $L^2\bar{\rho}_{3D}$, where L is the length unit), and the density contrast $\delta(x)$ is defined as $\delta(x) = (\varrho(x) - \bar{\varrho})/\bar{\varrho}$. The space coordinate x is assumed to be comoving with the cosmological background.

The Fourier transform of the density δ is denoted by $\tilde{\delta}(k)$. The power spectrum $P(k)$ of the primordial perturbations of the initial density field is defined as:

$$P(k) = |\tilde{\delta}_k|^2. \quad (2.1)$$

It is assumed to be a power-law in k :

$$P(k) \propto k^n. \quad (2.2)$$

If the spectral index n is larger than -1 the gravitational evolution of structures follows a hierarchical pattern, smaller structures collapsing before larger ones. In the following, the cases $n = 0$ and 1 will be considered.

A. Inverse collapse times in 1D

The gravitational evolution of a cosmological pressureless fluid can be described as a map from an initial, quasi-homogeneous configuration to an evolved one:

$$x(q, t) = q + S(q, t). \quad (2.3)$$

Here q is the initial, Lagrangian (comoving) coordinate of a fluid element, x is its final, Eulerian (comoving) location at the time t , and S is called the displacement field. For small displacements, the map S can be expressed as a perturbative series [7–9], whose first-order term gives the well known Zel'dovich (1970) [18] approximation²:

$$S(q, t) = -b(t)\nabla_q\varphi(q). \quad (2.4)$$

Here $b(t)$ is the growing mode for linear perturbations [3], which is equal to the scale factor $a(t)$ in an Einstein-de Sitter background cosmology, and φ is the initial peculiar rescaled gravitational potential, which obeys the equation:

$$\nabla_q^2\varphi(q) = \delta(q, t_i)/b(t_i) \equiv \delta_l. \quad (2.5)$$

The quantity δ_l , which is the initial density contrast linearly extrapolated to the present time, is called the linear density.

In 1D, the first-order term of the Lagrangian perturbation series gives the exact solution of the equations of motion up to OC, where the map in Eq. 2.3 becomes multi-valued. The density contrast can be expressed as:

$$1 + \delta(q, t) = 1/(\partial x/\partial q) = 1/(1 - b(t)\delta_l(q)). \quad (2.6)$$

In this case δ_l takes the role played by the three eigenvalues λ_i of the deformation tensor $S_{a,b}$ in 3D (recall that the sum of the three λ_i gives δ_l), and $J(q, t) = \partial x/\partial q$ is the Jacobian determinant of the $q \rightarrow x$ transformation.

It was shown by Monaco (1995; 1997a,b [26,10,11]) that the MF can be constructed on the basis of the inverse of the collapse ‘times’ $F \equiv b(t_c)^{-1}$, where the growing mode is used as a time variable. The collapse time t_c is defined as the instant at which the density goes to infinity and is found from the solution of the following equation:

$$J(q, t_c) = \partial x/\partial q = 0. \quad (2.7)$$

² The first-order term gives the Zel'dovich approximation only for a limited (but mostly used) set of initial conditions; see Buchert (1992) [25].

From Eq. 2.6 it follows that:

$$F(q) = \delta_l(q). \quad (2.8)$$

In other words, the 1D dynamical MF is based on the linear density contrast, which is assumed to be a Gaussian random field.

A very similar inverse collapse time is obtained if it is assumed that perturbations evolve according to linear theory, and that collapse takes place if the linear density is greater than a threshold density δ_c :

$$F_{\text{lin}}(q) = \frac{\delta_l(q)}{\delta_c}. \quad (2.9)$$

The fact that the Zel'dovich and linear inverse collapse times are proportional does not mean that the two descriptions are equivalent. Indeed, the use of the Zel'dovich approximation allows a clear definition of collapse as OC, while the definition remains vague in linear theory. Moreover, the Zel'dovich approximation fixes the value of the δ_c parameter to be one, thus leaving no free parameters. Notably, as this method is exact up to OC, the same result is obtained if 1D ‘spherical collapse’ is used to determine the parameter δ_c , as usually done in the 3D case.

B. Excursion set approach

Eq. 2.8 shows that the dynamical inverse collapse time in 1D is the Gaussian linear density field. It follows that the 1D MF can be constructed by means of the usual PS approach, based on linear theory. In more detail, the MF is correctly described by the extended PS theory, also known as the excursion set approach, proposed by PH [21] and Bond et al. (1991) [22].

The reason for introducing the excursion set approach is the following. In the perturbative schemes, and for power spectra that have power at all scales (like the ones given by Eq. 2.2 with $n > -1$), it is necessary to smooth the initial conditions to remove the small scale power which would go highly non-linear. This procedure is valid under the hypothesis that the dynamics of the smaller scales that are removed by smoothing do not affect strongly the behavior of larger scales [27]. Then the dynamical prediction of collapse is based on the linear density field smoothed with a filter $W_R(q)$ on a hierarchy of scales R . The ‘resolution’ of the smoothed field will be denoted in the following both by the smoothing radius R and by the mass variance Λ :

$$\Lambda = \langle (\delta_l * W_R)^2 \rangle. \quad (2.10)$$

Here the asterisk denotes a convolution. The mass variance Λ is usually denoted by the symbol σ^2 , which is not used here because it is misleading to use a squared quantity as an independent variable. If the power spectrum is a power law, R and Λ are connected as follows: $\Lambda = (R/R_0)^{(1+n)}$, where n is the spectral index and R_0 is the radius corresponding to unity mass variance.

The excursion set formalism is based on the idea that if a point is predicted to collapse at the resolution Λ (radius R), then it must be considered as collapsed at any larger resolutions (smaller radii), because the introduction of information from smaller scales cannot reverse collapse. The MF problem can be recast into one of scattering trajectories (in the F - Λ plane; see Bond et al. 1991 [22]) with an absorbing barrier at $F = F_c$, where

$$F_c = 1/b(t). \quad (2.11)$$

The fraction of trajectories absorbed by the barrier at resolutions smaller than Λ (or at radii larger than R) gives the fraction of mass collapsed at that resolution; this quantity is denoted by $\Omega(< \Lambda)$, and its Λ -derivative by $\omega(\Lambda)$ ³. The mathematical nature of the problem, and hence its solution, depends critically on the shape of the window function W_R . If W_R is a sharp low-pass filter in the Fourier space (sharp k -space filter, hereafter SKS), then the trajectories are random walks, and the absorbing barrier problem becomes a diffusion problem, which can be solved through a Fokker-Planck equation. The solution turns out to be the usual, correctly normalized PS formula

$$\omega(\Lambda)d\Lambda = \frac{F_c}{\sqrt{2\pi\Lambda^3}} \exp\left(-\frac{F_c^2}{2\Lambda}\right) d\Lambda. \quad (2.12)$$

³Note that, in the case of an Einstein-de Sitter universe, for which the density parameter Ω is unity, $\Omega(< \Lambda)$ is the contribution to the cosmological density coming from collapsed objects at the resolution $< \Lambda$.

If the smoothing is not SKS, the diffusion is subject to a complex colored noise, and the absorbing barrier problem cannot be solved exactly. However, PH have developed a useful approximation to determine the fraction of collapsed mass; this is given in their Eq.

$$\omega(\Lambda) = \left[\frac{\exp(-1/2\Lambda)}{\sqrt{8\pi\Lambda^3}} - \int_{-\infty}^1 P_F(x, \Lambda) dx \times \right. \\ \left. \frac{1}{\pi\Lambda_c \ln 2} \ln \left(\int_{-\infty}^1 P_F(x, \Lambda) dx \right) \right] \times \\ \exp \left[\int_0^\Lambda \ln \left(\int_{-\infty}^1 P_F(x, \Lambda') dx \right) \frac{d\Lambda'}{\pi\Lambda_c \ln 2} \right]. \quad (2.13)$$

Here P_F is the probability distribution function (hereafter PDF) of F , i.e. a Gaussian with zero mean and variance Λ , and $\Lambda_c = 2\Lambda\gamma(1 - \gamma^2)^{-1/2}$ is a correlation length for trajectories (the standard spectral measure γ is defined in in PH).

The freedom in the choice of the shape of the window function, and the different resulting MFs, is one of the most annoying aspects of the extended PS theory. Given that filtering is introduced in order to solve for the dynamics in the mildly non-linear regime, the shape of the window function must be chosen so as best to reproduce the exact dynamical evolution of the density field. This is in the same spirit as the optimization of the truncated Zel'dovich approximation [28]. In this sense, Gaussian smoothing is expected to be preferable.

The transformation from the resolution variable Λ or R to the mass variable M is where the geometry of the collapsed structures enters into the MF theory. The knowledge of the fraction of mass collapsed at a resolution is not enough to determine how the mass gathers into well-defined clumps. It is reasonable to expect that the mean size of the clumps is proportional to the smoothing radius, which is the only typical length present in the problem (as long as the power spectrum is scale-free or gently curved). Then, an order-of-magnitude estimate of the mean mass of the clumps is given by:

$$M = \text{const} \times \bar{\rho} R. \quad (2.14)$$

The exact proportionality constant depends on the shape of the smoothing window; it is a reasonable choice to keep it as a free parameter, as in Lacey & Cole (1994) [29]. With the transformation given in Eq. 2.14, it is possible to express the MF $n(M)$ through the following ‘golden rule’ (as named by Cavaliere, Colafrancesco & Scaramella 1991 [30]):

$$Mn(M)dM = \bar{\rho}\omega(\Lambda) \left| \frac{d\Lambda}{dM} \right| dM. \quad (2.15)$$

In practice, a whole distribution of masses forms at a given resolution; as argued by Monaco (1997b) [11], the actual MF will be a convolution of Eq. 2.12 or Eq. 2.13 with some distribution of masses formed at a given radius. To determine this distribution one should evaluate the size of the extended patches of Lagrangian space whose mass elements gather into a collapsed clump. The excursion set approach cannot be used for this purpose because mass elements are treated at the 1-point level, neglecting any spatial correlation between them. A solution of this geometrical problem thus requires an extension of the formalism. We propose a simple semi-analytical solution.

C. From resolution to mass

To determine the masses which form at a given resolution, it is useful to construct a function $R_c(q)^4$, that gives, for each point q of the Lagrangian space, the largest collapsing radius at which the point is predicted to collapse (in other words, at which its trajectory upcrosses the F_c barrier for the first time). This function is very useful because it contains in a compact way all the multi-scale information relevant for the MF problem. Fig. 1 shows a typical $R_c(q)$ curve⁵ for a realization of a scale-free spectrum with $n = 0$ (see Section III.A for more details). The intersection of

⁴ It is also possible to construct a function $\Lambda_c(q)$. The smoothing radius has been used because the resulting plots are easier to interpret and visualize.

⁵ Note that the $R_c(q)$ curve is smooth, the step-like appearance is an artifact.

this curve with a line of constant radius R defines a set of segments; these give the simply connected regions of points in Lagrangian space that are collapsed at radii $\geq R$. Under the reasonable assumption that each simply-connected collapsed region gathers into a single collapsed object, the length of each segment (times $\bar{\rho}$) gives the mass of the object at the radius R . Due to the solution of the cloud-in-cloud problem, the excursion sets, and then object masses, can only grow with decreasing R . It is very important to note that, although object masses depend on the smoothing radius, for each object there exists an interval of radius for which the mass does not change much. A reasonable definition of the mass of a clump should be independent of the smoothing radius R , which is a spurious quantity introduced in the theory because we are not able to solve the full dynamical problem. Then, the stabilization with R of the mass M of structures allows it to be defined in a meaningful way.

It is possible to construct, for each object, a growth curve $M_i(R; M_{\text{sat}})$, which gives the mass M of the i -th object at radius R , saturating at M_{sat} . These curves are not defined for all R values, as objects appear at some radius and are nested to other objects at some other smaller radius (this is not a merging event, as R is not a time variable). In the limit of infinite variance, all points collapse, and then all the structures percolate into one. This is not worrisome in cases analogous to that shown in Fig. 1, where the mass of each object is well defined for a significant range in radius.

The growth curves for objects with mass in an infinitesimal interval around M_{sat} can be averaged as follows:

$$\langle M_i(R; M_{\text{sat}}) \rangle = M_{\text{sat}} G(R; M_{\text{sat}}). \quad (2.16)$$

It is assumed that the mean growth curve does not depend on M_{sat} ; we have verified the validity of this assumption in our analysis. It is convenient to recast the saturating mass in term of a ‘saturating radius’, which is defined as

$$\text{const} \times R_{\text{sat}} = M_{\text{sat}} / \bar{\rho}. \quad (2.17)$$

The value of the constant in this equation is discussed below.

The total mass collapsed at radius R in a large volume V (in Lagrangian space) is given by a sum over all the $M_i(R)$, the contributions given at R by all the objects contained in the volume. The abundance of objects with mass M_{sat} is given by the MF $n(M)$ evaluated at M_{sat} . Then, as $\bar{\rho}V$ is the total mass contained in V , in the limit of infinite volume the fraction of collapsed mass is

$$\Omega(> R) = \frac{1}{\bar{\rho}} \int_0^\infty M_{\text{sat}} n(M_{\text{sat}}) G(R; R_{\text{sat}}) dM_{\text{sat}}. \quad (2.18)$$

It is possible to write Eq. 2.18 as a convolution. To this aim, it is convenient to use the mass variance Λ as resolution variable, and to express the mass M_{sat} in terms of a variable $\Lambda_{\text{sat}} = \Lambda(R_{\text{sat}})$, where $R_{\text{sat}}(M_{\text{sat}})$ is given by Eq. 2.17. Under the hypothesis of mass-independence, the function G is expressible as a function of $\Lambda/\Lambda_{\text{sat}}$. We define the function $\tilde{\omega}(\Lambda)$ as the one satisfying the ‘golden rule’ relation:

$$M(\Lambda) n(M(\Lambda)) dM(\Lambda) = \bar{\rho} \tilde{\omega}(\Lambda) \left| \frac{dM}{d\Lambda} \right|^{-1} dM(\Lambda). \quad (2.19)$$

The $M(\Lambda)$ function is the inverse of $\Lambda_{\text{sat}}(M_{\text{sat}})$ and the differential fraction of collapsed mass $\omega(\Lambda)$ is

$$\Lambda \omega(\Lambda) d \ln \Lambda = \left[\int_{-\infty}^{\infty} \Lambda_{\text{sat}} \tilde{\omega}(\Lambda_{\text{sat}}) \frac{dG}{d \ln \Lambda} (\ln \Lambda - \ln \Lambda_{\text{sat}}) d \ln \Lambda_{\text{sat}} \right] d \ln \Lambda. \quad (2.20)$$

In other words, the logarithmic derivative of the fraction of collapsed mass is the convolution of the $\tilde{\omega}(\Lambda)$ function, which satisfies the golden rule, with the logarithmic derivative of the mean growth curve for the objects.

The golden rule is recovered in the case in which G is a step function, and $dG/d \ln \Lambda = \delta^D(\Lambda - \Lambda_{\text{sat}})$, where δ^D is a Dirac delta function. This would correspond to an R_c curve made up by a collection of rectangles, whose heights are proportional to their widths. The golden rule can give a fair approximation to the MF as long as the logarithmic derivative of G is sharply peaked, and as long as the constant in Eq. 2.17 makes the peak coincide with $\Lambda/\Lambda_{\text{sat}} = 1$. Reversing the argument, the position of the peak of the $dG/d \ln \Lambda$ curve gives the best constant to use in Eq. 2.17. As a consequence, it is not necessary to give the exact constant of proportionality between radius and mass, as the deconvolution from the differential growth curve will select the best one; no free parameters are present in this MF theory. In the following, the ‘Gaussian’ value $\sqrt{2\pi}$ will be used both for Gaussian and SKS smoothing.

III. SIMULATIONS

A. Description of Simulations

To investigate the dynamics of the cosmic fluid in 1D, we wrote a PM *Particle-Mesh* code [13,12] to follow the non-linear evolution of perturbations. The PM method of integration has been preferred over other methods, such as PP (*Particle-Particle*), P³M (*Particle-Particle/Particle-Mesh*), or TreeCode, because it is considerably faster, and in one spatial dimension it can reach a satisfactory resolution by using a large number of grid points. The lack of precision of the PM integration for distances smaller than the grid spacing is not important for our purposes, as we are not interested in the individual properties of the trajectories of each fluid element [14].

The code integrates the standard Vlasov-Poisson equation for a collisionless, self gravitating cold fluid in an expanding framework of coordinates, using a particle sampling of a given initial density perturbation field. The framework is defined as $r = a(t)x$, where r is the physical coordinate and $a(t)$ and x are, as before, the expansion factor and the comoving coordinate. As discussed at the beginning of Section II, the expansion has been chosen to follow the Einstein-De Sitter model for a flat universe. The one-dimensional Vlasov-Poisson equations are given and discussed, e.g., in Doroshkevich et al (1980) [13]. The Poisson equation is integrated as usual in Fourier space, taking advantage of the FFT algorithm. We use a CIC (*Cloud-In-Cells* [14,12]) smoothing algorithm for assigning the mass of the particles to the grid points and for interpolating the force from the grid points to the particles. The velocities and positions of the particles are evaluated using a time-centered leap-frog scheme, with time-dependent coefficients that account for the simultaneous expansion of the comoving framework of coordinates [14,12].

The force acting upon the particles is constant, and depends only on the amount of matter (i.e. on the number of particles) present on the right and the left of each particle. In one dimension, the direct calculation of the forces would be thus exact, so that a PP integrator could have some advantage with respect to the PM one. But, if a good resolution in mass is requested, the PP integrator too time-expensive, and the PM scheme is preferable.

The initial conditions for all the simulations have been given consistently with the linear theory of the evolution of perturbations. The particle sampling of the density perturbation field is obtained using the Zel'dovich approximation that has been shown to generate a particle distribution that well reproduces the given power spectrum [12].

We tested the code by comparing the analytical linear evolution of a single-wavenumber perturbation with the numerical integration of the same perturbation. Furthermore, we compared the mildly nonlinear evolution of various density perturbation fields with the results obtained using the Zel'dovich approximation, which in this case is exact till OC. We also included in the code checks of the conservation of the energy, obtained in comoving coordinates using the Layzer-Irvine equation [3], and of the conservation of linear momentum. The code also checks the maximum shift of any particle in one time step.

As mentioned above, we consider initially scale-free spectra $P(k) \propto k^n$ for the initial density perturbation field (Eq. 2.2), with $n = 0$ and 1. In these cases, perturbations in the initial density contrast field are present at all scales of the simulation, their relative power depending upon the spectral index. The normalization of a scale-free power spectrum is somewhat arbitrary; we attach a comoving ‘physical’ length to the simulation segment, setting it to $L_{box} = 1000h^{-1}Mpc$, and normalize in the ‘standard’ way by defining a smoothed variance, filtered with a top-hat filter at a scale $R_{TH} = L_{box}/10$, and linearly evolved to $a_0 = 1$, as

$$\Lambda_{TH}(a_0, R_{TH}) = \frac{1}{2\pi} \int P(k) W^{TH}(kR_{TH}) dk = 1, \quad (3.1)$$

where $W^{TH}(kR)$ is the Fourier transform of a 1-dimensional top-hat filter, and $a_0 = 1$ is the normalization of the expansion factor. The initial time of the simulations has been chosen to correspond to the epoch a_{in} when the density fluctuations on the Nyquist scale are equal to the white noise level; therefore the initial epoch of the simulation are different for the two different spectral indices, while the differences in output times among the simulations belonging to the same spectral index depend on the interference among the various random amplitudes at different k values. We note that the *physical* initial conditions and intermediate outputs of all the simulations are equivalent, since they are defined using the variances and not the simulation times.

For each spectral index, we have performed ten simulations with different random Fourier phases. The same seed for the random number generator has been given to the simulation code when running with different spectra, so that the two sets of ten simulations and different spectral indices have the same phases. The final epoch for all simulations is $a(t) = 1.0$. One of the simulation for each spectral index (the first one) has a perturbation amplitude *equal* to the power spectrum, while the others have Gaussian-distributed amplitudes with *variance* given by $P(k)$ at the scale k . Thus, one of the simulations for each spectral index is equivalent to an ensemble average over many different realizations of the initial conditions. Each simulation has a number of particles $N_p = 524288$ and a number of grid-points $N_{gr} = 262144$, with a grid space length of $l = 0.0038h^{-1}Mpc$. We have five order of magnitude of resolution in

length, and four times more in mass. The non-conservation of energy is always smaller than 1%; important bulk flows are not observed and the total linear momentum is exactly conserved, at the numerical error level. The maximum shift of a particle in a time-step is never greater than $0.8l$. The number of time-steps used for each simulation is $N_{st} = 19000$. For each simulation we have ten outputs, roughly linearly spaced in time, corresponding to linearly extrapolated variances $\Lambda_{TH} \simeq 0.0028, 0.0174, 0.0562, 0.135, 0.225, 0.335, 0.468, 0.623, 0.801$ and 1 (top-hat smoothing on $1/10$ of the box is again assumed).

B. Negative Jacobian and Multi-Streaming

A key point in comparing the dynamical MF theory to simulations, already raised by Monaco (1997a) [10], is that the clump-finding algorithm must seek those structures that are actually predicted to form by the theory. In the present case, the clump-finding algorithm must look for connected multi-stream regions at a certain scale. In fact, a large density contrast is a consequence, due to the continuity function, of OC and multi streaming. Standard clump-finding algorithms based on percolation or on overdensities, such as the friend-of-friends (hereafter FOF) one or others seeking density peaks, may not be the best choice for finding multi-stream regions, because they typically find them in a biased way. This is the case in 3D; more compact, roundish clumps are typically preferred over filamentary or sheet-like structures (even by FOF if the linking length is chosen so as to pick up the virialized clumps), making such algorithms unsuitable for the comparison with a theoretical prediction based on OC and multi streaming. Moreover, standard clump-finding algorithms have a free parameter, like the FOF linking length or a threshold density, while our theoretical predictions do not.

When searching for multi-stream regions, a difficulty immediately appears. Fig. 2 shows the x vs q plot of a simple Gaussian perturbation: the triple-valued region, in which triplets of different elements q get to the same Eulerian point x , is the multi-stream region. The slope of the $x(q)$ curve gives the Jacobian determinant of the transformation. The ‘OC’ condition of having a negative Jacobian, Eq. 2.7, is then satisfied for those points q where the slope of the curve is negative. This defines a segment in Lagrangian space which is shorter than the whole multi-stream region. In the following, these regions will be called NJ regions, while the whole multi-stream regions will be called MS regions.

The origin of the problem is that mass elements which have a negative Jacobian according to the Zel’dovich approximation are subject to OC and get shocked only after crossing the structure. However, the Zel’dovich approximation is not a good tool for describing the behavior of mass elements subject to multi-streaming: after entering an MS region, the mass element starts to interact highly non-linearly and non-locally with the other mass elements, without waiting a whole crossing time to be shocked. Then, the Zel’dovich approximation is not able to recover the whole MS region, which is nevertheless dynamically relevant. On the other hand, it can be a fair approximation to say that the NJ collapse condition finds mass elements that have approximately first-crossed an MS region. If MS regions were infinitely thin, such as in the adhesion theory, then there would be no difference between them and NJ ones. So this problem is connected to the finite width of MS regions. As long as the density around caustics shows some kind of universal profile [19,31], one expects a tight correlation between the masses of MS- and NJ-based objects.

To find the NJ and MS regions in the simulation, the Eulerian positions of particles have been evaluated on a mesh grid in Lagrangian space, made up by 65536 grid points, through a CIC interpolation. The resulting $x(q)$ curve has been smoothed with a hierarchy of Gaussian filters of decreasing radius R . NJ regions have been identified with connected regions (segments) characterized by a negative slope of the $x(q)$ curve, while MS regions have been identified with connected regions of points in triple-valued regions. This algorithm is fast, easy to implement and does not contain free parameters. Its multi-scale nature is analogous to the multi-scale nature of the MF problem; as a consequence it is possible to construct $R_c(q)$ curves (like the one shown in Fig. 1) for the NJ or MS regions in the simulations by recording the largest smoothing radius R_c at which the particle at grid point q enters an NJ or MS region. As in Section II.C, it is possible to construct growth curves for the R -dependent objects, defined as segments in the intersection of the R_c curve with a line of constant R , and the mass of these objects is well defined as long as the growth curves for the objects saturate at some value.

The definition of structure proposed here is different from more standard ones, although the continuity equation assures that both MS and NJ regions are tightly related to high-density clumps. The importance of the algorithm described above relies on its connection with the important dynamical concepts of NJ and MS: the NJ and MS structures are important regardless how they compare to clumps defined in more standard ways. Moreover, the performance of standard clump-finding algorithms has not been thoroughly tested in the 1D case, which is remarkably different from 3D in many regards. As a consequence, we will focus mainly on the NJ and MS structures, as their analysis allows us to deepen the dynamical problem and develop many useful techniques extendable to the 3D case. Anyway, a comparison of NJ and MS structures to FOF clumps will be shown in Section IV.D for completeness.

IV. COMPARISON OF THEORIES WITH SIMULATIONS

The $R_c(q)$ curves, as the one shown in Fig. 1, have been constructed from the analytical predictions of collapse, both with Gaussian (GAU) and SKS smoothing, applied to the initial conditions of the simulations described in Section III.A, resampled on a grid in Lagrangian space with 65536 grid points. In the SKS case, it is necessary to follow all the modes of the box to sample the F trajectories in all the points; to keep the analysis feasible, only the first 10000 modes have been considered. Analogous $R_c(q)$ curves have been found by seeking NJ and MS regions in the simulations, as described in Section III.B.

Fig. 3 shows the $R_c(q)$ curves for the third output of the first simulation, both with $n = 0$ and $n = 1$ (the third output is chosen as it is the first one in which the differential growth curve is stable; at the NJ and MS level, it shows more structure than the following ones). Only one tenth of the box is shown. In particular, Figs. 3a and 3c show a comparison of GAU and NJ curves, Figs. 3b and 3d a comparison of the SKS and MS curves. Some important points can be appreciated from a visual inspection of Fig. 3:

1. The theoretical predictions based on Gaussian smoothing are able to reproduce accurately the NJ regions in the simulations (Figs. 3a and 3c). A cross check with Figs. 3b and 3d shows that SKS structures are systematically larger than GAU ones. It is confirmed that Gaussian smoothing optimizes the dynamical prediction of NJ.
2. Surprisingly, SKS predictions reproduce, although not with great accuracy, the MS regions (Figs. 3b and 3d). This ‘coincidence’ is due to the fact that the SKS smoothing overestimates the size of GAU collapsed regions nearly as much as the MS regions overestimate the size of the NJ regions.
3. SKS and MS structures tend to include more than one GAU or NJ structure.
4. All structures, especially NJ and GAU ones, show a general tendency toward saturation.
5. The agreement of theory and simulations is better for $n = 0$ than for $n = 1$. This is expected, as $n = 1$ gives more small-scale power, which provides, through highly non-linear dynamics, noise in the predictions relative to larger scales.

In the following subsections all the conclusions just drawn are statistically quantified. Section IV.A gives a global analysis of the $R_c(q)$ curves, Section IV.B gives object-by-object comparisons, Section IV.C shows the resulting MFs and Section IV.D shows a comparison with FOF objects.

A. Global Analysis

Three statistics are used to quantify the agreement between different $R_c(q)$ curves: the coincidence statistic, which is based on counting points for which two different predictions agree or disagree, the Pearson and the Spearman correlation coefficients. The comparison of two R_c curves is done by cutting the curves to progressively larger radii, so as to test the effect of small scale objects.

The coincidence statistic is defined as follows. We count the number of points in the Lagrangian grid for which neither, one or both curves predict collapse. The number of points for which neither of the two curves predicts collapse results of minor interest, as at large R -values it is dominated by the large number of points which have not collapsed. The statistic chosen for the comparison is the ratio between the number of points for which both curves predict collapse and the number of points for which at least one of the two give collapse. In formal terms, the coincidence statistic is defined as follows:

$$C = \frac{P(R_{c1}(q) > R_{cut} \text{ AND } R_{c2}(q) > R_{cut})}{P(R_{c1}(q) > R_{cut} \text{ OR } R_{c2}(q) > R_{cut})}. \quad (4.1)$$

Here R_{c1} and R_{c2} are the two curves being compared, $P(\text{event})$ denotes the probability of the event within the brackets, and R_{cut} is the cut in smoothing radius. The coefficient C takes values from 0 (anti-coincidence) to 1 (perfect coincidence).

The correlation of two R_c curves is also measured by means of two standard statistical indicators, the Pearson linear coefficient r_p and the Spearman non-parametric rank coefficient r_s [32].

Fig. 4 shows the three correlation coefficients C , r_p and r_s for the pairs of curves shown in Fig. 3 (the results for the other simulations are similar). The agreement between GAU and NJ curves is good at all scales, with correlation coefficients larger than 0.8 in the $n = 0$ case; the agreement is still present but worse in the $n = 1$ case. The agreement

between SKS and MS curves is not as good, but a strong correlation is still present at all scales, with correlation coefficients always in excess of 0.6. Note that the increase of the coincidence coefficient C in Figs. 4b and 4d is artificial: the SKS predictions are not pushed to very small radii, and this lack of small structures mimics a real lack of small MS objects.

B. Object-by-object analysis

An object is defined, at a given smoothing scale R , as a segment defined by the intersection of the $R_c(q)$ curve with a line of constant R . The growth curves G for objects are constructed as follows. Two segments at R and $R - \Delta R$ are considered part of the same growth curve when the one at $R - \Delta R$ includes the one at R (segments at R cannot be partially included in segments at $R - \Delta R$). Two growth curves are nested if they end up in the same segment; in this case the growth curve corresponding to the smaller object is stopped, while the larger one takes the mass of both structures and continues growing. A growth curve is considered as saturated when its mass changes by not more than 5% for a change of R by a factor 1.3. It has been verified that the catalogues of objects and their statistical properties do not change significantly when the saturation conditions are slightly changed. The saturating mass of the object M_{sat} is calculated as the average mass within the central half of the R -interval of saturation.

Some objects fail to saturate; these are in general small objects, whose growth curves have not saturated at the smallest radius considered in the analysis or have been nested to a larger object. In this case the object is assigned the mass at its smallest radius. Such objects are considered in the analysis, but not to construct the final growth curve.

After saturation, growth curves continue to grow by accreting small or tiny objects. As all the objects end up percolating at some small scale, it is very important to define the mass of objects at their first saturation. However, the mass which is further acquired by the objects is not assigned to any smaller clump. This highlights a problem with the definition of isolated clumps; any uncertainty in the definition of larger clumps is at the expenses of smaller ones. The choice made here of neglecting the mass further accreted by the object can lead to a decrease of the number of small mass objects. However, there is no reason to believe that assigning this mass to small objects would be a better choice.

The comparison of two different object catalogues is done by associating the objects in one catalogue with the ones in the other catalogue if their associated segments at the saturation mass intersect. An object of a catalogue can thus be associated with more than one object in the other catalogue. In fact, most of these associations are between objects of quite different sizes. It is interesting to consider the average number of objects in catalogue B associated with a single object in catalogue A, which will be denoted by \bar{n}_{AB} , and the same average number limited to those objects whose mass is at least 10% of the mass of the object they are associated with, denoted by $\bar{n}_{AB}^{10\%}$. We have also considered the fraction of mass of the largest and second largest objects in catalogue B, in terms of the mass of the object in catalogue A with which they are associated, which will be denoted by $M2/M1_{AB}$ (if there is not a second largest object, its mass has been set to 0). This quantity is important; if it is small, the MF is likely not to be severely affected by a disagreement at the object-by-object level. Note that all these quantities change if the A and B catalogues are commuted; then, the pairs of catalogues have been compared in both senses.

Fig. 5 shows these three quantities for pairs of catalogues of all the objects found in all the outputs of all the simulations. Masses are rescaled to the value of M_* , and the results are shown in four bins of M/M_* . The comparisons shown are again GAU vs NJ and SKS vs MS, in both the $n = 0$ and $n = 1$ cases. The results obtained by inverting the two catalogues considered are also shown, except for the $M2/M1_{AB}$ indicator, which does not change much on inverting the catalogues.

The comparison of GAU and NJ catalogues is shown in Figs. 5a and 5c. Although NJ regions tend to include many small GAU structures, especially for $n = 1$, the number of ‘large’ associated objects is not much different from one. The $M2/M1_{AB}$ index is always smaller than 0.1, indicating that the second associated objects are negligible in terms of mass. As before, the two catalogues agree more in the $n = 0$ case.

The comparison of the SKS and MS catalogues, shown in Figs. 5b and 5d, reveals a good object-by-object agreement, although not as good as that of GAU and NJ objects. In particular, SKS objects tend to include many MS objects at large masses, but again the mass of the second associated object is almost negligible.

Fig. 6 shows a one-to-one comparison of the masses of associated objects, in units of M_* . All the objects of the third output of all the simulations are shown. The masses refer to the pair of largest associated objects; then, only a subset of all the objects is shown. The masses show a tight correlation in all cases, which is tighter for $n = 0$. The correlation is almost unbiased, even though objects found from simulations tend to be more massive than predicted.

In conclusion, the catalogues extracted from simulations with the NJ or MS algorithms reveal a good agreement with the ones predicted with GAU or SKS filters. It is then demonstrated that in 1D the dynamical MF theory agrees

with the simulations on an object-by-object basis, once the clump-finding algorithm is designed to find exactly what is sought for. The agreement worsens if the spectral index n is larger, so that more small-scale power is present in the spectrum.

C. Mass Functions

In Section II.C it was shown that to obtain the MF, the fraction of collapsed mass $\Omega(< \Lambda)$ must be deconvolved from the mean growth curve of objects. The mean growth curve is constructed by averaging the single growth curves described in the last subsection. The independent variable for the growth curves is given by the logarithm of the ratio between the two variances Λ and Λ_{sat} , corresponding respectively to the smoothing radius R and the radius R_{sat} which corresponds to the total mass M_{sat} of the object through Eq. 2.17. The average is performed over all saturated objects in all the ten simulations, at fixed output time. It has been verified that the resulting mean growth curve does not depend on the output time. In more detail, the first two outputs show somewhat different growth curves, as the objects are still small and their growth curves are not sampled well enough. The results shown and used in the following are those relating again to the third output.

Figs. 7 shows the mean integral and differential growth curves for GAU and SKS objects, for the two spectra considered. As discussed in Section IV.B, objects continue their growth after saturation. Consequently, the mean growth curves do not saturate exactly at unity. The differential growth curve is truncated so as to be properly normalized. The differential growth curves show a prominent peak. The peak position is different for the GAU and SKS curves, showing that the SKS curve requires a larger constant in Eq. 2.17. The peaking of the differential growth curves confirms that the golden rule can be a good approximation for estimating the masses of the objects. The position of the peak depends on the spectrum, for the GAU filter it decreases with n increasing (the consequences of this will be discussed in the Conclusions). The $n = 0$ curves are more sharply peaked than the $n = 1$ curves. The SKS curves are much more noisy, especially at small variances. This is a consequence of the nasty oscillations of the SKS filter in real space.

Fig. 7 shows also the $\omega(\Lambda)$ curves, given in Eq. 2.12 and Eq. 2.13, and those deconvolved from the differential growth curve ($\tilde{\omega}(\Lambda_{\text{sat}})$, Eq. 2.20). The deconvolution is performed numerically; this is a delicate and unstable calculation, such that the large-mass part of the mass function can be spoiled by numerical oscillations, especially in the SKS case, where the small-variance tail of the differential growth curve is very noisy. However, the numerical deconvolution turns out to be satisfactory in the GAU case.

The excursion set formalism is able to predict, through Eqs. 2.12 and 2.13, the integral ($\Omega(< \Lambda)$) or differential ($\omega(\Lambda)$) fraction of mass collapsed at a variance Λ . This prediction is exact for SKS filters, and a good approximation for Gaussian filters, and hence we expect to find a very good agreement between the analytical and semi-analytical curves (i.e. obtained from the GAU and SKS R_c curves). The accuracy of the agreement between analytical and semi-analytical predictions gives then a measure of the fluctuations present in the initial conditions of the simulation especially at large scales, due to the power-law nature of the power spectra used. These fluctuations are enhanced in the simulation by the non-linear coupling of the first two modes of the box. The effect of this non-linear coupling is also seen in Fig. 3, where the R_c curves taken from the simulations are systematically higher than the analytical curves. In other realizations, where the first two modes interact destructively, the numerical curves tend to be lower than the analytical ones. As long as this enhancement does not influence the width of the spikes in Fig. 3, neither the catalogues of objects nor their MF is going to be strongly affected by this effect, which is however revealed by analyzing the fraction of collapsed mass $\Omega(< \Lambda)$.

We have found that at least ten simulations are necessary to average out these large-scale fluctuations. Large masses, or small variances, remain affected by the fluctuations as they are determined by a few objects per simulation. Fig. 8 shows the comparison of the analytical (PS and PH), semi-analytical (GAU and SKS) and numerical (NJ and MS) $\Omega(< \Lambda)$ curves, for $n = 0$ and $n = 1$; the third output of all simulations is used. The analytical and semi-analytical curves agree well, as expected. Some disagreement is present at small variance, due to shot noise, and in the comparison between the GAU and PH curves, due to the approximate nature of the PH analytical prediction when Gaussian filters are used. The $\Omega(< \Lambda)$ curves from the simulations show strong fluctuations at small variance, and a tendency to predict more collapsed mass, which is consistent with the slightly larger masses of the objects from the simulations, visible in Fig. 6. The agreement with the analytical and semi-analytical curves is good at moderate and large variance for $n = 0$, but is not satisfactory for $n = 1$. From a more detailed analysis of the simulations, which is not shown for reasons of brevity, it appears that this behavior is caused by the non-linear coupling of small and large-scale modes, which is stronger with $n = 1$ than with $n = 0$, and causes the large-scale fluctuations to influence small scales.

In the scale-free cases analyzed in this paper, the MFs at different outputs can be rescaled by showing the quantity

$M_* n (M/M_*) dM/M_*$. Due to the resolution and statistical limits, every output samples a different part of the mass function, so that a good range in mass can be achieved by using all the outputs. Constructing a mass function from a weighted average of all the outputs is not correct in principle, as the outputs are not independent. However, showing the results of many different outputs is quite confusing. For this reason we perform an average, weighted by the number of objects in the bin, of the MFs from different outputs, with the *caveat* that this procedure is motivated mainly by graphical reasons. Fig. 9 shows the GAU, SKS, NJ and MS MFs of all the outputs, together with the averaged ones. The stability of the averaging procedure is apparent.

The MFs shown in Fig. 9 are compared in Fig. 10. The analytical predictions of PS and PH are shown, both those obtained with the standard golden rule (with Gaussian mass) and those obtained with the deconvolution procedure of Section II.C. The following points can be noted:

1. The GAU and NJ mass functions are in very good agreement. Consistent with what was found above, the NJ curve tends to give more massive object, and is slightly flatter (for $n = 0$) at smaller masses.
2. The deconvolved PH curve improves significantly the agreement between the analytical and semi-analytical GAU curves, confirming the validity of the deconvolution procedure of Section II.C. The residual disagreement at large masses is probably motivated by the fact that the large mass part of the GAU MF is mainly determined by the first output, for which the growth curves are not well sampled. The small-mass slope is fairly well reproduced, implying that the mass neglected by the clump-finding algorithm does not influence significantly the MF in the mass range tested.
3. The agreement between the SKS and MS MFs is very good. The deconvolution does not greatly improve the agreement between the analytical and semi-analytical predictions, because of the difficulty in determining a good mean growth curve for the SKS objects.
4. Both the SKS and MS MFs tend to cut off at small masses. This is an artifact in the SKS case, as small smoothing radii are not considered, but it is real in the MS case, as large MS regions tend to include the smaller ones.
5. Consistent with what was found above, the results with $n = 1$ are worse than those with $n = 0$.

It is worth noting that no free parameters are involved in the comparison of the different MFs.

D. Friends-of-friends groups

The clump-finding algorithm developed in this paper has been constructed to reproduce the NJ and MS regions in Lagrangian space. Moreover, this algorithm is based on the saturation condition for the growth curves, which, as shown in Section IV.C, is not exactly achieved, and this can lead to a decrease of small-mass objects. In this sense the algorithm, although physically motivated, may be considered not ideal for general application.

Standard clump-finding algorithms are typically applied to the evolved configuration of a simulation in Eulerian space. Such algorithms are designed to select simply connected clumps (like the friends-of-friends one, hereafter FOF [33]) or high-density peaks (DENMAX, SKID [34], HOP [35] or SO [36] ones). These algorithms have been developed and tested for analyzing 3D simulations, but generally have not been used in 1D. Therefore, the use of such algorithms in our case is not guaranteed to lead to reliable results. We have nevertheless decided to analyze our simulations with the standard and most frequently used FOF algorithm, in order to compare its performance to our OC-based one.

With the FOF algorithm, groups are defined as those sets of particles whose distance from at least another member of the group is smaller than a given linking length. In 3D, it is usual to set this linking length to 0.2 times the average interparticle distance; in this way the selected groups have an overdensity of at least ~ 180 , which corresponds to the density contrast of a spherical virialized clump. In 1D this argument does not hold, and therefore we have left the linking length as a free parameter, fixing it as that which gives a mass function which best resembles the other numerical ones. A compromise value of 1.5 times the mean interparticle distance has been used. In this way the FOF MF reproduces the large-mass end MS MF for $n = 0$ and the NJ MF for $n = 1$. We have checked that moderate variations of the linking length lead to similar results. Remarkably, the value of the linking length used is larger than that used in 3D. This can be explained by the fact that 1D clumps, having a more limited number of degrees of freedom, do not relax and virialize as easily as in 3D. As a consequence their internal distribution has a larger amount of substructure, made up of the caustic fronts which are generated by multi-streaming. Then, a larger linking length is necessary not to fragment the multi-streaming regions. This highlights the fact that 1D FOF clumps are remarkably different from 3D ones.

A basic prediction of the mass function theory is that structures correspond to simply connected regions in the Lagrangian space. For an appropriate comparison of the FOF mass function with the other ones presented above, in which structures are defined as segments in q -space, it is necessary to verify that this hypothesis holds for the FOF clumps (which are by construction connected only in the x -space). To check this, we have calculated, for each FOF clump found from the output of a simulation, the Lagrangian distance between two particles (starting from the median particle) which contain a fixed fraction of mass. If the clump is simply connected (it is a segment in the q -space), and if the mass is expressed in units of comoving length (with $\bar{\rho} = 1$), the two quantities (distance and fraction of mass) would be equal. An estimate of the connectivity of the clumps is then given by the fraction of mass (in unit of Lagrangian length) of the clump included in the Lagrangian distance defined above, averaged over all the objects of a simulation. In fig. 11 we show this curve for the third output of the first realization of $n = 0$; other outputs give very similar results even for $n = 1$. If the hypothesis of simple connection held exactly, then the function would coincide with the bisector line shown in the Figure. It is apparent that the deviation from the simply connected hypothesis is not severe, especially in the inner parts of the clump, while the borders, which contain no more than 10% of the mass, are more fragmented.

However, the object-by-object comparison of the FOF and GAU or SKS catalogues of objects reveals a poor agreement, as shown in Fig. 12. The figure shows the results of performing the same analyses as described in Section IV.B and in Fig. 5 and 6, only for the case $n = 0$. The results for $n = 1$ are very similar. Figs. 12a and b show that significantly more than one object of a catalogue is associated with each object of the other catalogue, and that the second largest object is always significant in terms of mass. Figs. 12c and d show that the correlation between the largest companions is still significant but with a considerable scatter, much larger than the previous cases. The comparison between NJ and MS groups and FOF clumps is very similar, and is not shown, as we are not interested at this level in comparing different 1D clump-finding algorithms.

Fig. 13 shows the MFs of FOF groups compared with the ones shown in Fig. 10, for $n = 0$ and $n = 1$. Only the third output of the first realization is shown, as it is enough to make the point. In the $n = 0$ case the FOF MF is similar to the MS and SKS ones, but it is more peaked at $M = M_*$, and the small-mass slope is shallower. The peak at $M = M_*$ is even more evident in the $n = 1$ case, where the FOF MF cuts off similarly to the GAU and NJ ones. It is noteworthy that, by tuning the linking length, one could reproduce the large-mass cutoff of any of the other MFs, without changing much the (dis)agreement at the object-by-object level. Moreover, at variance with the 3D case, the linking length should change with the spectrum to reproduce the cutoff of either the GAU or the SKS MFs with different spectra.

As a conclusion, the analytical mass function does not reproduce well the FOF mass function of the simulation, both statistically and on an object-by-object base. In our opinion, the difference between this result and the standard 3D case arises predominantly from the different behavior of the FOF algorithm in 1D relatively to the widely tested 3D case.

V. SUMMARY AND CONCLUSIONS

In this paper we have shown a complete analysis, performed with analytical, semi-analytical and numerical techniques, of the cosmological MF problem with 1D gravity. When gravitational collapse is identified with the first crossing of the orbits, the dynamical solution of the MF problem, analogous to that reviewed by Monaco (1998) [4] for the 3D case, coincides formally with that of linear theory, but with no free parameters. Then, the MF is well described by the usual extended Press & Schechter theory [1,21,22]. The determination of the size of collapsed regions is performed by constructing (with semi-analytical techniques) a mean growth curve for the objects, which gives the distribution of masses that form at a given smoothing radius. The analytical MF is then determined by a deconvolution of the well known formulae of Press & Schechter [1] and Peacock & Heavens [21] from the mean growth curve.

To test the predictions of the MF theory, two sets of ten simulations of flat expanding universes have been performed. The two sets differ only in the power spectrum of primordial perturbations, which is assumed to be a power-law with index $n = 0$ or 1. The simulations have been analyzed by searching for the regions in the Lagrangian space which have a negative Jacobian (NJ) or are in the multi-stream regime (MS). The difference between NJ and MS regions arises as an effect of the finite size of MS regions. Notably, this kind of analysis is intrinsically multi-scale. The analytical predictions of collapse have been applied to the initial conditions of the simulations, in order to have semi-analytical predictions for the objects found in the simulations, and then to test the recovery of the MF object by object. To obtain such predictions, both Gaussian and sharp k -space smoothing filters have been used.

To characterize in a compact way the multi-scale collapse of the density field, we have introduced the function $R_c(q)$, which gives the largest smoothing radius at which the point q in Lagrangian space is predicted or ‘observed’ (in

the simulation) to collapse. The R_c curves have been constructed both for the semi-analytical predictions of collapse and for the NJ and MS regions found in the simulations. The semi-analytical predictions of collapse have then been tested by comparing the R_c curves; the agreement has been quantified by using several correlation indices. Catalogues of objects have been defined starting from the R_c curves, and exploiting the tendency of simply connected collapsed regions in Lagrangian space to be stable for a range of smoothing radii. In this way the definition of object becomes effectively independent of the resolution at which the density field is filtered. The semi-analytical and simulated catalogues of objects have been compared both on an object-by-object basis, using several indices to quantify the agreement, and statistically, by comparing the resulting MFs.

The overall result is that the dynamical MF theory in 1D is able to reproduce the collapsed objects in the simulation both statistically and object by object, once the clump-finding algorithm applied to the outputs of the simulation is designed so as to find the objects which are in fact predicted, i.e. the NJ or MS regions. In more detail, Gaussian smoothing allows an optimal reconstruction of NJ regions, as anticipated by Monaco (1997a,b) [10,11], while the objects found with SKS smoothing resemble the MS regions. The good agreement is reached without tuning any free parameter. As expected, the agreement is better if the spectral index is $n = 0$, because in the $n = 1$ case the small-scale power present enhances the effect of highly non-linear dynamics, which is simply removed in the analytical and semi-analytical predictions. If the standard friends-of-friends algorithm is used to define the collapsed clumps in the simulations, then the agreement is much worse, especially at the object-by-object level. However, the performance of the friends-of-friends algorithm has not been thoroughly tested in 1D.

The analyses presented in this paper have shown that the solution of the mass function problem in 1D is important for understanding the dynamics of gravitational collapse, as its degree of complexity is high enough to be interesting, but low enough to be fully manageable. The results of this paper are then useful to address the 3D case. However, the 3D problem presents several important complications, so that the relevance of the simple 1D study is not obvious.

Firstly, while in 1D the Zel'dovich approximation is exact up to OC, in 3D further-order terms in the Lagrangian perturbation theory must be considered. However, it was shown by Monaco (1997a) [10] that the Lagrangian series converges in predicting the collapse of mass elements, provided that it is not too slow. Pushing the calculations to third order is enough to achieve a satisfactory degree of precision in the dynamical prediction of collapse, at least for the large-mass part of the mass function.

Secondly, in 3D the mass elements are subject to collapse along three different directions, so that it is in principle possible to define either a “first” collapse along the first axis, or a collapse along the second or the third axis. First-axis collapse does not separate fully-virialized clumps and pancake-like or filamentary transients, so that third-axis collapse could be a better choice for isolating virialized halos [37,38]. The difference between the two cases is well illustrated in the collapse of a spherical peak which has a decreasing density profile [4]: all mass elements except the central one are subject to cylindrical symmetry, and never collapse along the third axis. Then, collapse along the third axis is able to pick up the seeds for structure formation, and works well if applied, for instance, to the peaks of the density field (as done, e.g., by Bond & Myers 1996 [37]), but it is not a good choice for recovering all the collapsing mass. The fact that Lee & Shandarin (1998) [38] need a fudge factor of 12.5 to achieve a good normalization for their mass function can be seen as a consequence of this fact.

Thirdly, while the collapsed field in 1D remains separated in simply-connected regions down to large variance, the 3D collapsed field percolates at moderate variance. In other words, the excursion sets of the $R_c(\mathbf{q})$ field in 3D soon become geometrically and topologically complex. There is need of a further criterion to fragment the collapsed medium into objects; such criterion could for instance be based on the peaks of the $R_c(\mathbf{q})$ field. Only after this criterion is defined, it is possible to construct the growing curve for the objects. This is related to the important (and not trivial) problem of assessing the relation between regions in the multi-stream regime (either NJ or MS) and the clumps found by standard algorithms. We stress again that, whatever the result, the NJ or MS regions are interesting by themselves, because of their dynamical meaning.

An analysis of 3D simulation is in progress, and some preliminary results have already been presented in Monaco (1999) [40]. The $R_c(\mathbf{q})$ curves have been calculated, using Gaussian smoothing, for a realization of a Gaussian field on a cubic grid, used as initial condition for a numerical P³M simulation. The $\mathbf{x}(\mathbf{q})$ map from the simulation has been smoothed and differentiated, so as to calculate the Jacobian determinant in each point and then find the NJ regions. The agreement between predictions and NJ regions is good as expected. Further analyses show an encouraging similarity between NJ regions and FOF groups, mapped in the Lagrangian space, at variance with the 1D case. As discussed in the text, the NJ condition peaks up the collapsed points only after their first crossing of the structure, and this helps in excluding the less relaxed regions. The fragmentation of the collapsed medium cannot be uniquely defined [40], and this is related to the fact that there is not a unique clump-finding algorithm.

Finally, we want to stress the importance of the concept of the mean growth curve, which allows the solution of a long-standing problem of the MF, namely that of a realistic (and simple!) treatment of the geometry and topology of collapsed structures in the MF theory. In section IV.C (see Fig. 7) it is suggested that the relation between resolution and mass can change with the spectral index, as when more small-scale power is present, the excursion sets are more

fragmented. If confirmed in the 3D case, this would explain the change of the δ_c parameter detected in the simulations of Governato et al. (1998) [39].

ACKNOWLEDGMENTS

The authors thank Annalisa Bracco, Paolo Catelan, Vince Eke, Antonello Provenzale and Tom Theuns for many discussions, and the anonymous referee for his comments. P.M. thanks George Efstathiou for his advice and support, and the Trans-Edit Group of Milano for hospitality. P.M. has been supported by the EC TMR Marie Curie grant ERB FMB ICT961709.

-
- [1] W. H. Press and P. Schechter, *Astrophys. J.* **187**, 425 (1974)
 - [2] for a review of this theory see, e.g., P. Coles and F. Lucchin, *The origin and evolution of cosmic structure*, (Wiley, New York, 1996)
 - [3] P. J. E. Peebles, *The Large Scale Structure of the Universe* (Princeton University Press, Princeton, 1980)
 - [4] P. Monaco, *Fund Cosm Phys* **19**, 153 (1998)
 - [5] A. G. Doroshkevich, *Astrofizika* **3**, 175 (1967)
 - [6] F. Moutarde, J. M. Alimi, F. R. Bouchet, R. Pellat and A. Ramani, *Astrophys. J.* **382**, 377 (1991); F. R. Bouchet, R. Juszkiewicz, S. Colombi and R. Pellat, *Astrophys. J.* **394**, 5L (1992); T. Buchert and J. Ehlers, *Mon. Not. R. Astron. Soc.* **264**, 375 (1993); see also the reviews by T. Buchert, in *Dark Matter in the Universe*, edited by S. Bonometto, J. Primack and A. Provenzale (1997); and F. R. Bouchet, in *Dark Matter in the Universe*, edited by S. Bonometto, J. Primack and A. Provenzale (1997)
 - [7] T. Buchert, *Mon. Not. R. Astron. Soc.* **267**, 811 (1994)
 - [8] F. R. Bouchet, S. Colombi, E. Hivon and R. Juszkiewicz, *Astron. Astrophys.* **296**, 575 (1995)
 - [9] P. Catelan, *Mon. Not. R. Astron. Soc.* **276**, 115 (1995)
 - [10] P. Monaco, *Mon. Not. R. Astron. Soc.* **287**, 753 (1997a)
 - [11] P. Monaco, *Mon. Not. R. Astron. Soc.* **290**, 439 (1997b)
 - [12] G. Efstathiou, M. Davis, C. S. Frenk and S. D. M. White, *Astrophys. J. Supp.* **57**, 241 (1985)
 - [13] A. G. Doroshkevich, E. V. Kotok, I. D. Novikov, A. N. Polyudov, S. F. Shandarin and Yu. S. Sigov, *Mon. Not. R. Astron. Soc.* **192**, 321 (1980)
 - [14] for a review of numerical codes used in Cosmology, see e.g. R. W. Hockney and J. W. Eastwood, *Computer Simulation Using Particles* (McGraw-Hill, New York, 1981); E. Bertschinger and J. M. Gelb, *Computers in Physics* **mar/apr 1991**, 164 (1991)
 - [15] S. N. Gurbatov, A. I. Saichev and S. F. Shandarin, *Mon. Not. R. Astron. Soc.* **236**, 385 (1989)
 - [16] A. G. Doroshkevich and T. V. Kotok, *Mon. Not. R. Astron. Soc.* **246**, 10 (1990)
 - [17] B. G. Williams, A. F. Heavens, J. A. Peacock and S. F. Shandarin, *Mon. Not. R. Astron. Soc.* **250**, 458 (1991)
 - [18] Ya. B. Zel'dovich, *Astrofizika* **6**, 319 (1970); translation: *Astrophysics* **6**, 164 (1973)
 - [19] S. F. Shandarin and Ya. B. Zel'dovich, *Rev. Mod. Phys.* **61**, 185 (1989)
 - [20] S. F. Shandarin, A. L. Melott, K. McDavitt, J. L. Pauls and J. Tinker, *Phys. Rev. L* **75**, 7 (1995)
 - [21] J. A. Peacock and A. F. Heavens, *Mon. Not. R. Astron. Soc.* **243**, 133 (1990)
 - [22] J. R. Bond, S. Cole, G. Efstathiou and N. Kaiser, *Astrophys. J.* **379**, 440 (1991)
 - [23] C. Lacey and S. Cole, *Mon. Not. R. Astron. Soc.* **262**, 627 (1993)
 - [24] see, e.g., C. Porciani, S. Matarrese, F. Lucchin and P. Catelan, *Mon. Not. R. Astron. Soc.* **298**, 1097 (1998)
 - [25] T. Buchert, *Mon. Not. R. Astron. Soc.* **254**, 729 (1992)
 - [26] P. Monaco, *Astrophys. J.* **447**, 23 (1995)
 - [27] For a proof see J. S. Bagla and T. Padmanabhan, *Mon. Not. R. Astron. Soc.* **286**, 1023 (1997)
 - [28] A. L. Melott, T. Pellman and S. F. Shandarin, *Mon. Not. R. Astron. Soc.* **269**, 626 (1994)
 - [29] C. Lacey and S. Cole, *Mon. Not. R. Astron. Soc.* **271**, 676 (1994)
 - [30] A. Cavaliere, S. Colafrancesco and R. Scaramella, *Astrophys. J.* **380**, 15 (1991)
 - [31] J. F. Navarro, C. S. Frenk and S. D. M. White, *Mon. Not. R. Astron. Soc.* **275**, 56 (1995)
 - [32] For a definition see, e.g., W. H. Press, S. A. Teukolsky, W. T. Vetterling and B. P. Flannery, *Numerical Recipes* (Cambridge University Press, Cambridge, 1992)
 - [33] M. Davis, G. Efstathiou, C. S. Frenk and S. D. M. White, *Astrophys. J.* **292**, 371 (1985)
 - [34] For DENMAX and SKID see <http://www-hpcc.astro.washington.edu/tools/>
 - [35] D. J. Eisenstein and P. Hut, *Astrophys. J.* **498**, 137 (1998)

- [36] see, e.g., A. Gardini, S. Bonometto and G. Murante, *Astrophys. J.*, submitted
- [37] R. J. Bond and S. T. Myers, *Astrophys. J. Supp.* **103**, 41 (1996)
- [38] J. Lee and S. F. Shandarin, *Astrophys. J.* **500**, 14 (1998)
- [39] F. Governato, A. Babul, T. Quinn, P. Tozzi, C. M. Baugh, N. Katz and G. Lake, *Mon. Not. R. Astron. Soc.*, submitted (astro-ph/9810189)
- [40] P. Monaco, in *The Development of Galaxy Systems*, edited by G. Giuricin et al., (ASP Conf. Ser, in press; astro-ph/9811085)

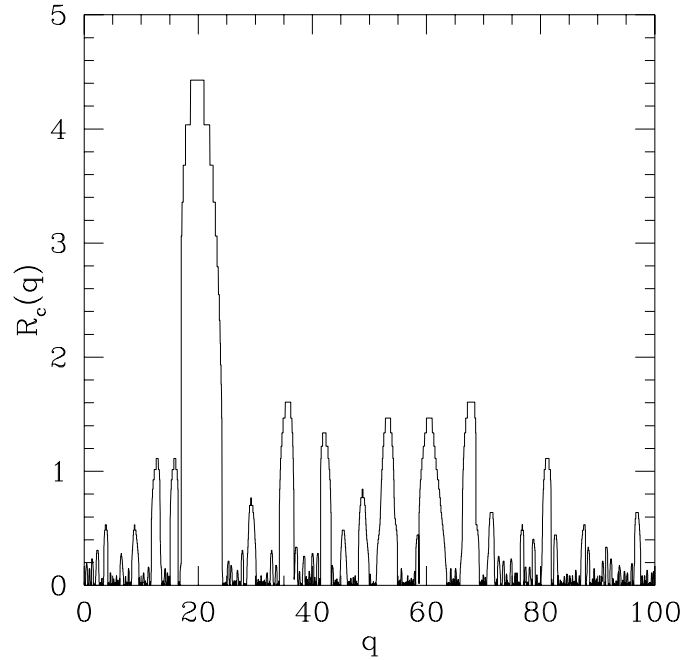


FIG. 1. $R_c(q)$, largest collapse radius as a function of q , for a realization of an $n = 0$ spectrum (Section III).

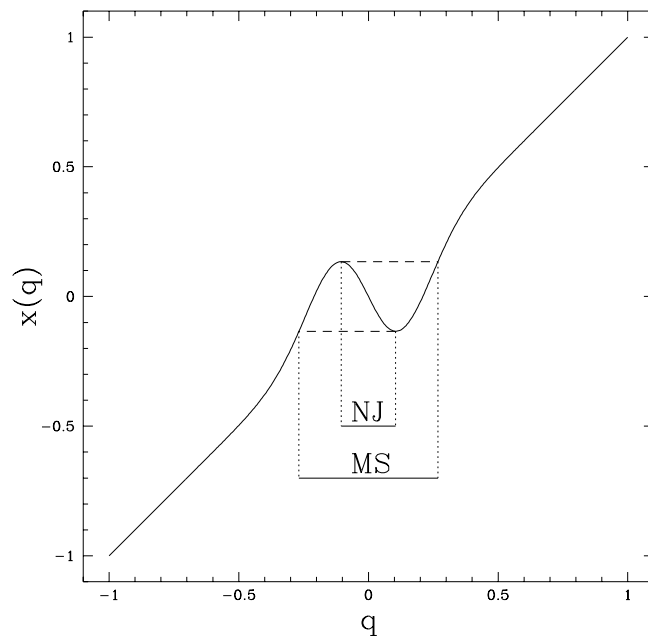


FIG. 2. Illustration of the difference between NJ and MS zones.

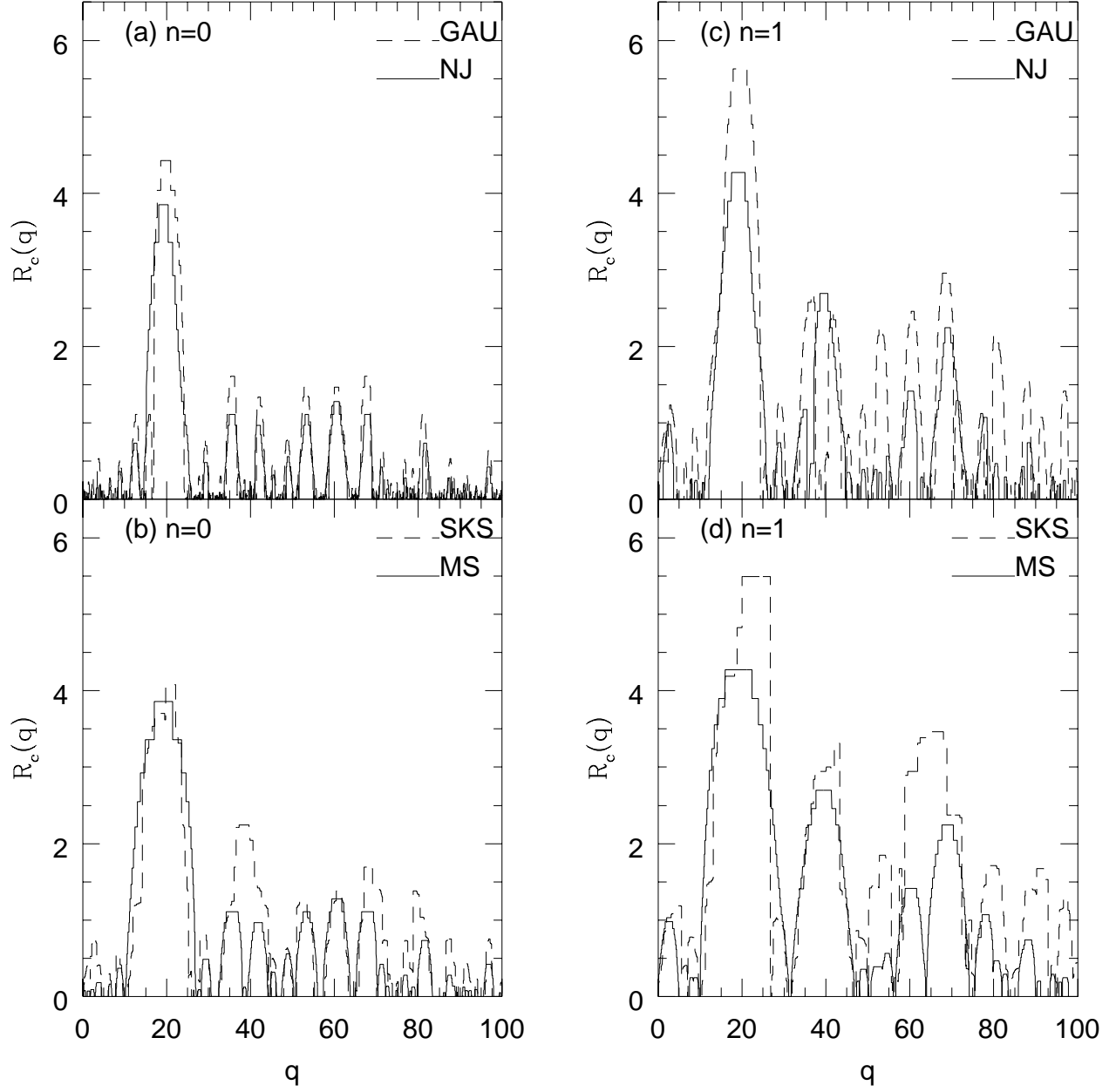


FIG. 3. $R_c(q)$ curves for different collapse definitions and different spectra

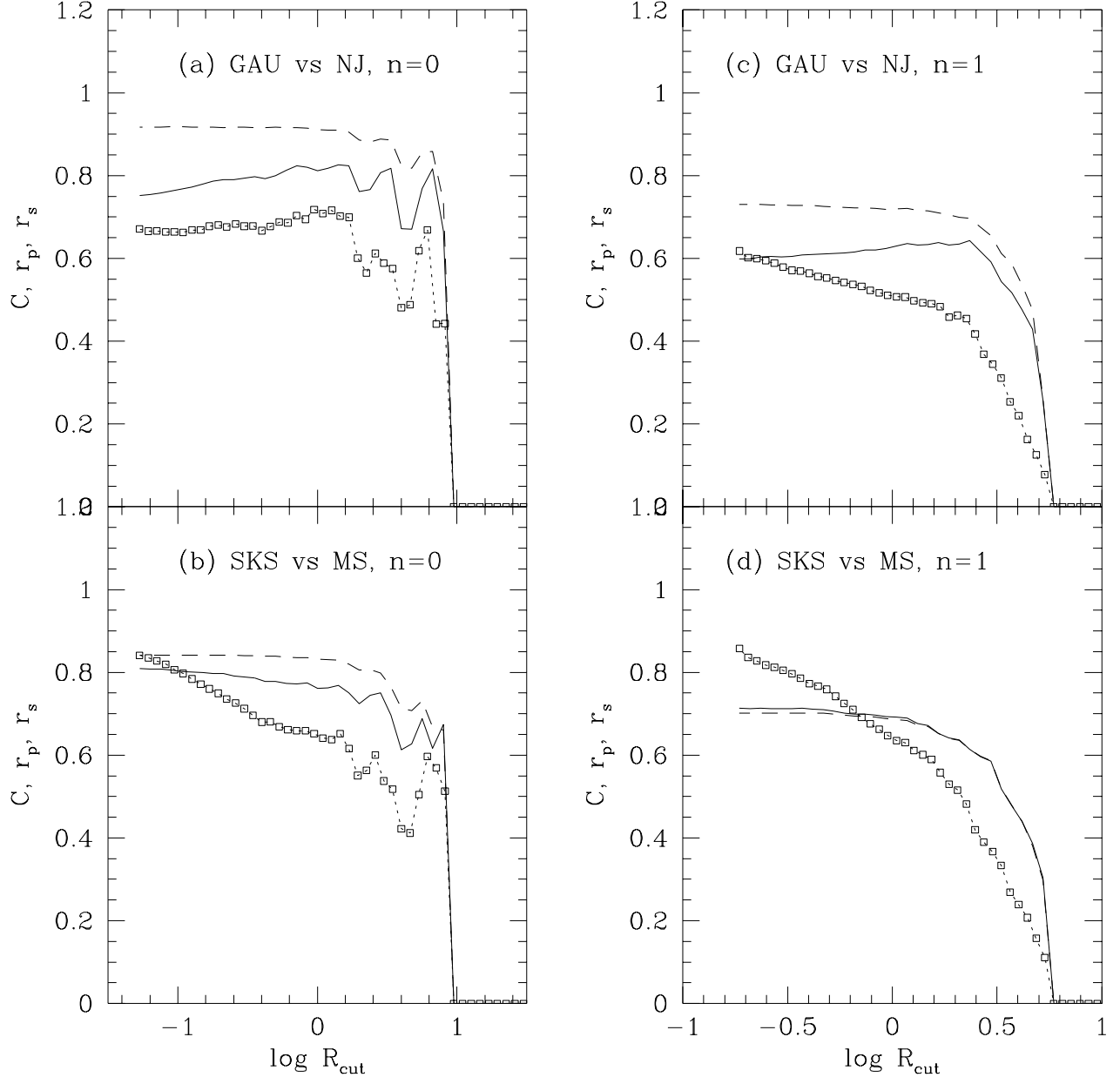


FIG. 4. Global correlations of different $R_c(q)$ curves. Dashed line: Spearman coefficient r_s . Continuous line: Pearson coefficient r_p . Dotted line with square points: coincidence statistics.

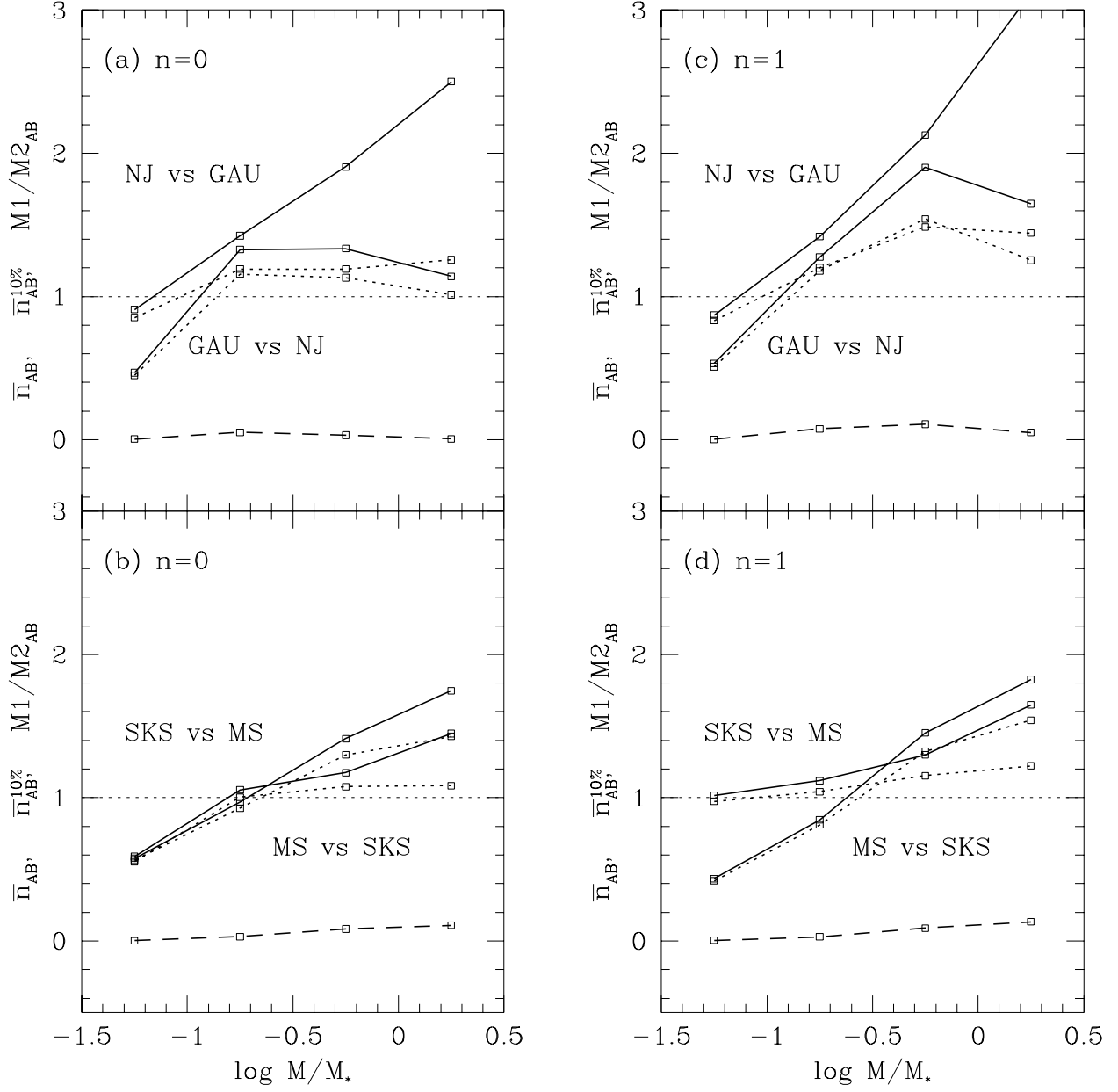


FIG. 5. Comparison of different catalogues of objects. Continuous line: \bar{n}_{AB} . Dotted line: $\bar{n}_{AB}^{10\%}$. Dashed line: $M2/M1_{AB}$

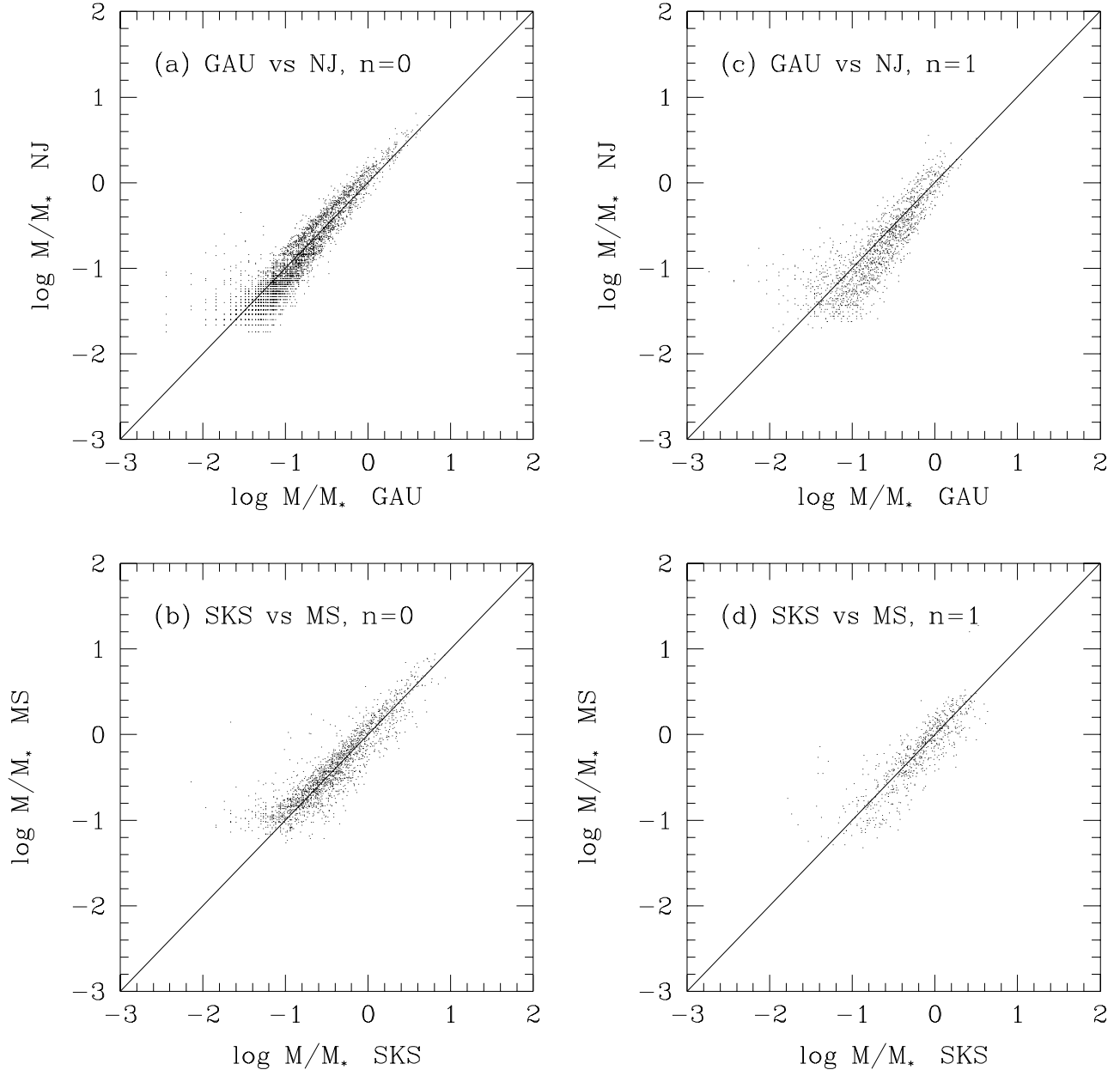


FIG. 6. Comparison of object masses.

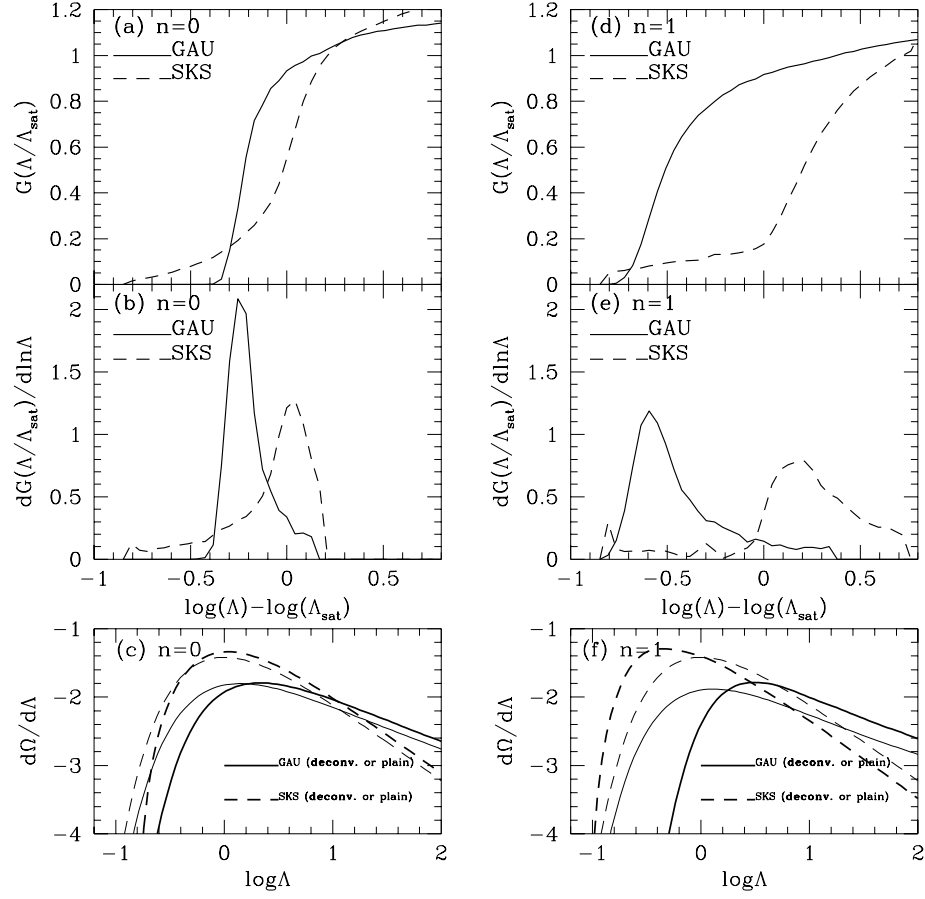


FIG. 7. Growth integral and differential curves; deconvolved $\omega(\Lambda)$ functions.

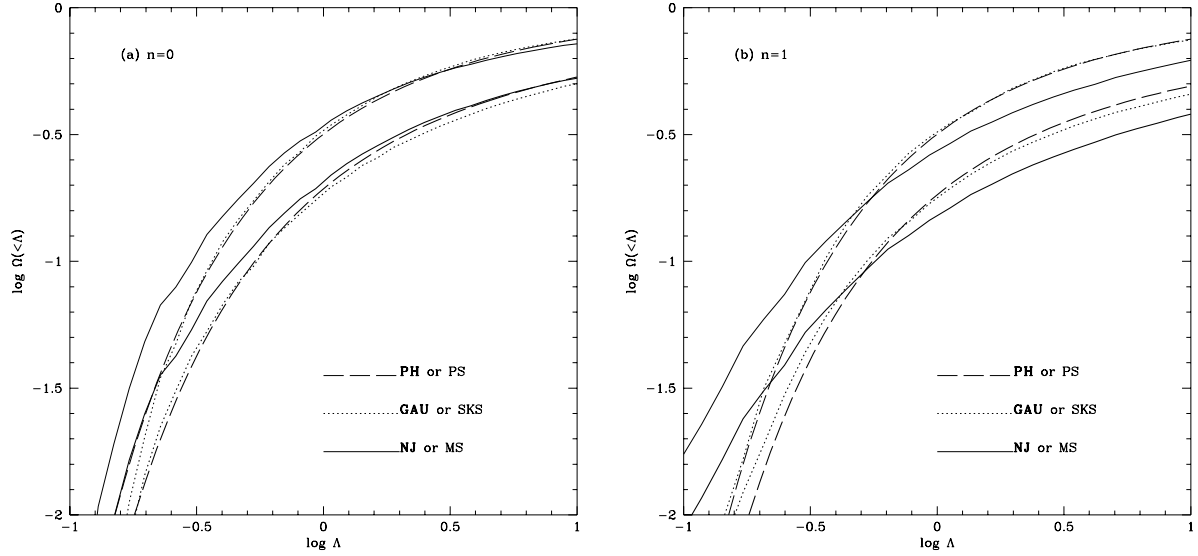


FIG. 8. Fraction of collapsed mass.

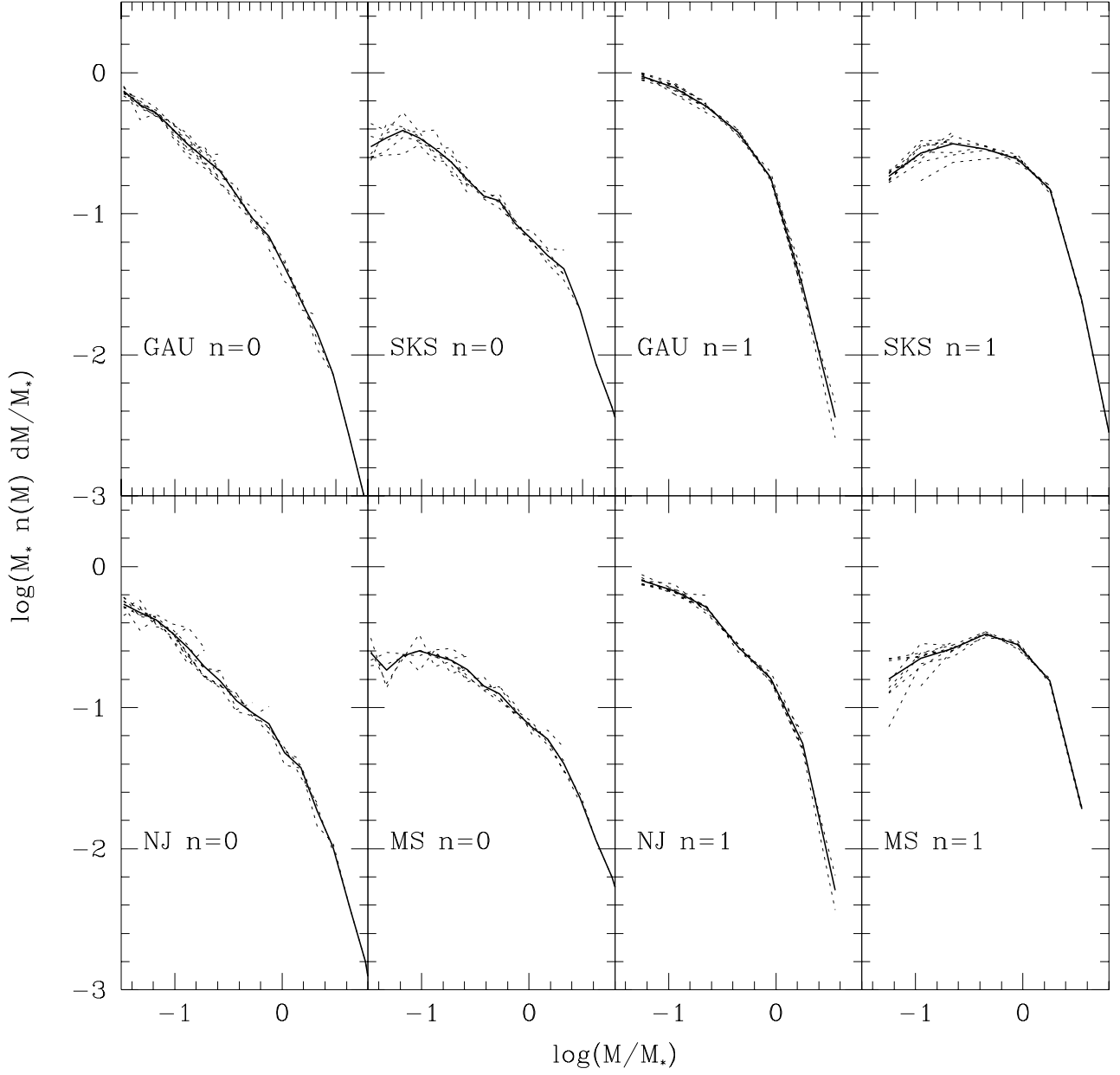


FIG. 9. Mass functions from different outputs: dashed lines represent single outputs, solid lines show the average.

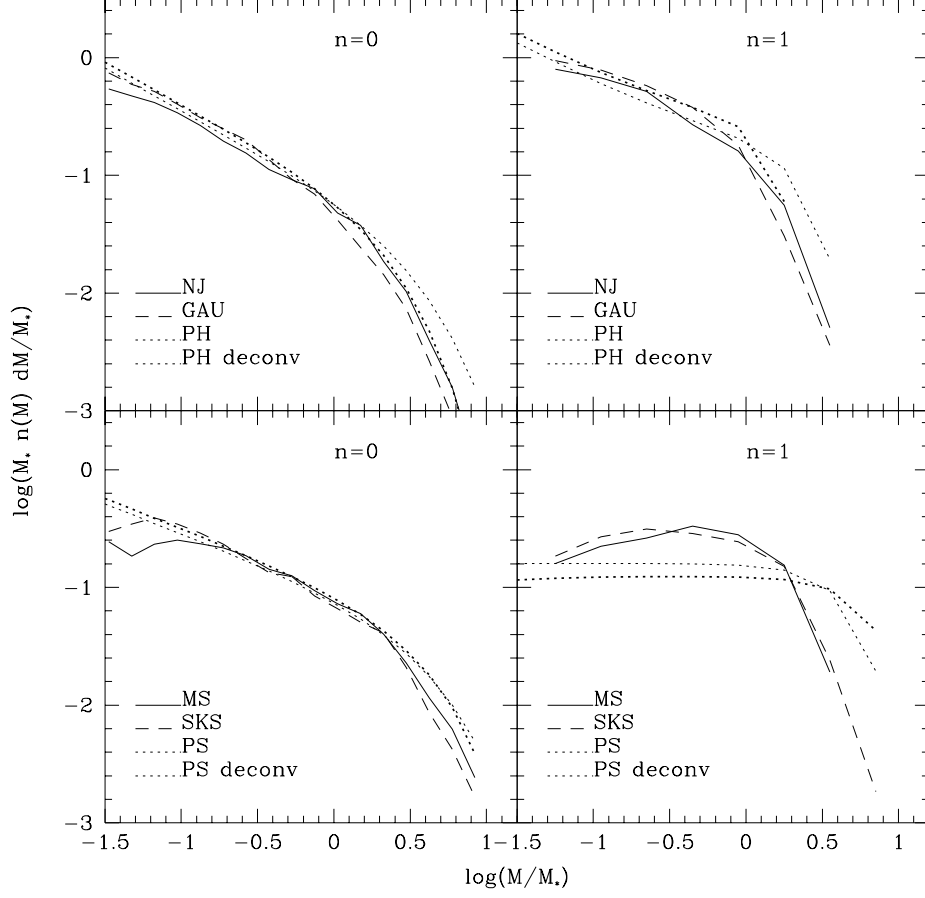


FIG. 10. Comparison of different mass functions.

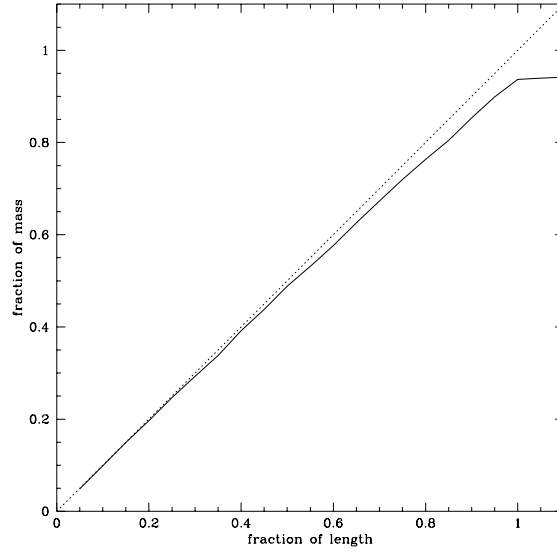


FIG. 11. Test of connectivity of FOF groups in Lagrangian space.

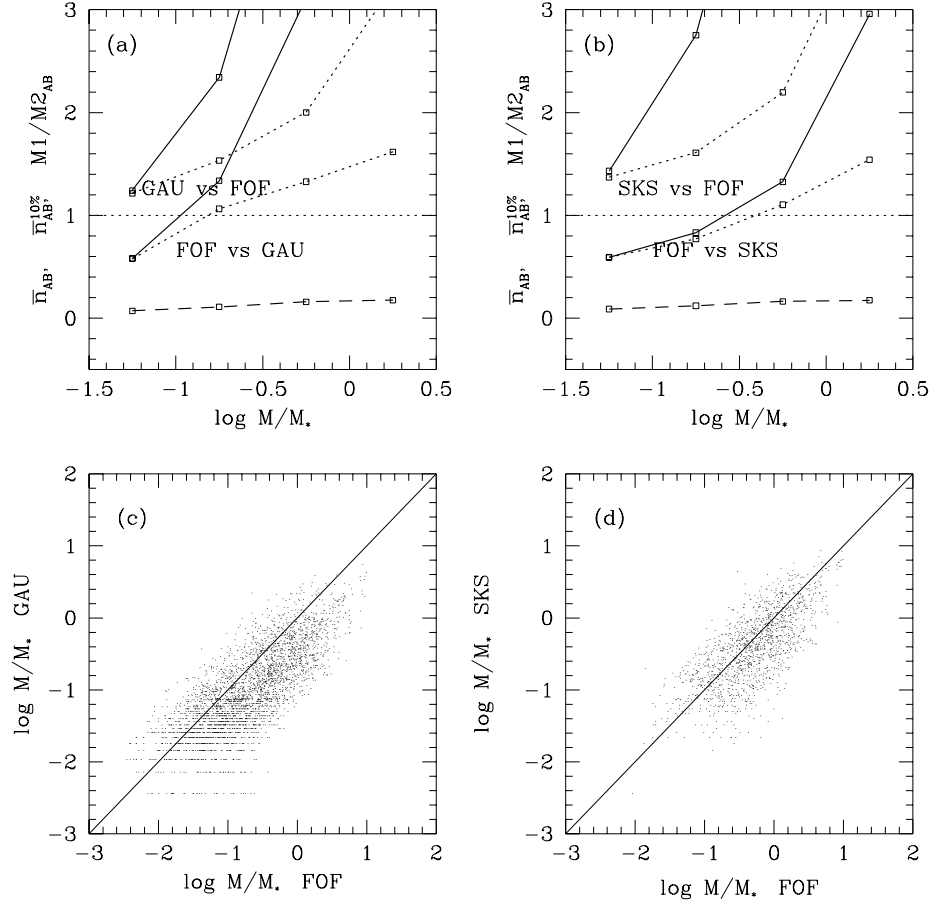


FIG. 12. Object-by-object comparison of FOF objects catalogues with GAU and SKS ones. In panels (a) and (b): continuous line: \bar{n}_{AB} . Dotted line: $\bar{n}_{AB}^{10\%}$. Dashed line: $M2/M1_{AB}$. Panels (c) and (d) show the correlation of the masses of associated objects.

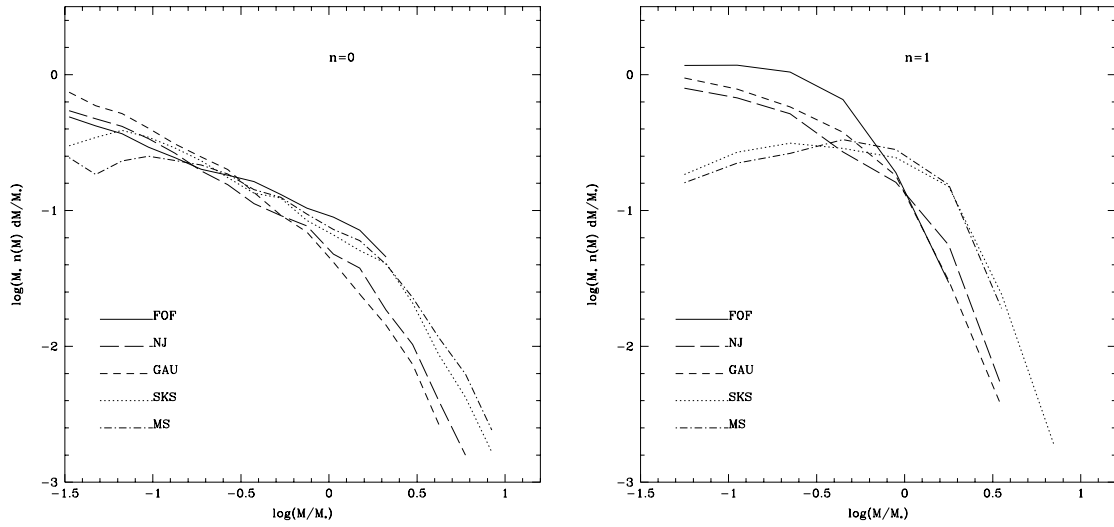


FIG. 13. FOF MFs compared to those of Fig. 10.